Int. J. Heat Mass Transfer. Vol. 30, No. 4, pp. 741–756, 1987
Printed in Great Britain

0017–9310/87 $3.00 + 0.00
Pergamon Journals Ltd.

Numerical study of natural convection in a tilted rectangular porous material

SARA L. MOYA and EDUARDO RAMOS

Laboratorio de Energía Solar, Instituto de Investigaciones en Materiales, Universidad Nacional Autónoma de México, 62580 Temixco, Mor., Mexico

and

MIHIR SEN†

Departamento de Fluidos y Térmica, Facultad de Ingeniería, Universidad Nacional Autónoma de México, 04510 México, D.F., Mexico

(*Received* 4 *February* 1985 *and in final form* 6 *August* 1986)

Abstract—Two-dimensional natural convective flow in a tilted rectangular porous material saturated with fluid is analyzed by solving numerically the mass, momentum and energy balance equations, using Darcy's law and the Boussinesq approximation. Isothermal boundary conditions are considered, where two opposite walls are kept at constant but different temperatures and the other two are thermally insulated. The external parameters considered are the tilt angle, the aspect ratio and the Darcy–Rayleigh number. Three main convective modes are found: conduction, single and multiple cell convection and their features described in detail. Local and global Nusselt numbers are presented as functions of the external parameters. Multiplicity of solutions is explored for aspect ratio unity. The existence of more than one solution is found when the bottom wall is at a higher temperature and in a horizontal or close to horizontal position.

1. INTRODUCTION

THERE ARE many applications of natural convection in porous media. For example, we may mention geothermal flows, insulation problems, nuclear engineering, petroleum extraction, storage of agricultural products, underground diffusion of contaminants and porous material regenerative heat exchangers. Due to its importance, a considerable amount of information already exists. A review of experimental and theoretical results up to 1975 is presented in an excellent paper by Combarnous and Bories [1].

In general, the flow pattern in porous media is fully three dimensional, but there is experimental evidence that under certain conditions, real flows show two-dimensional patterns. These are the cases we shall analyze in this paper. The particular conditions under which two-dimensional flows are observed will be discussed in detail below.

Consider a two-dimensional rectangular porous material with two opposite walls at constant but different temperatures, and the other two thermally insulated. The material will be said to be vertical, horizontal or tilted, depending on the orientation of its isothermal walls with respect to the gravity acceleration vector.

Most previous theoretical publications deal with horizontal [2–5] or vertical [6, 7] cases. Tilted rectangles have received less attention, one of the main contributions being made by Vlasuk [8] (reported in ref. [1]) who made a numerical integration of the governing equations and determined the heat transfer as a function of the tilt angle. An important result presented by him is that the tilt angle for maximum heat transfer for aspect ratio unity and Darcy–Rayleigh numbers in the 100–350 range, is approximately 50°. This effect also presents itself in a fluid filled cavity [9, 10], although the angle of maximum heat transfer is not necessarily the same. Holst and Aziz [11] made an investigation on the heat transfer of a tilted square porous material considering temperature-dependent physical properties. Weber [12] analyzed the problem of thermal convection in an infinite tilted porous layer using a perturbation technique. A Galerkin expansion was used by Walch and Dulieu [13] for a slightly inclined rectangular box. A correlation between the Nusselt number and the Darcy–Rayleigh number, the aspect ratio and the tilt angle was given. They have also identified the qualitative nature of the steady-state solutions as a cusp catastrophe [14]. Bifurcation and instability phenomena in porous material have received less attention, the first major work in this area being due to Lapwood [15], who found that the conductive solution for an infinite bottom-heated porous layer becomes unstable at $R = 4\pi^2$. Beck [16] extended these results to finite aspect ratios. Multiplicity of solutions in a tilted porous cavity has been studied numerically by Walch and Dulieu [14] and analytically by Caltagirone and Bories [17] who determined their stability.

† Present address: Department of Aerospace and Mechanical Engineering, University of Notre Dame, Notre Dame, IN 46556, U.S.A.

NOMENCLATURE

D	aspect ratio	W	width of the porous material
g	acceleration due to gravity	w	velocity in the stream tube direction
$\tilde{g}$	local component of gravity in stream tube direction	x, y	spatial coordinates.
H	height of the porous material	Greek symbols	
k	equivalent thermal diffusivity	α	tilt angle
K	permeability of porous medium	β	coefficient of volumetric expansion
L	total length of stream tube	η	spatial coordinate in the stream tube direction
$Nu(x)$	local Nusselt number		
$\overline{Nu}$	global Nusselt number	μ	dynamic viscosity of the saturating fluid
p'	pressure		
R	Darcy–Rayleigh number	ρ	fluid density
T	temperature	Ψ	stream function
T'_H, T'_C	temperature of hot and cold isothermal boundaries, respectively	Ψ_m	variable defined in equation (14).
u, v	velocity components in the x'- and y'-directions, respectively	Indices	
		$'$	dimensional variables
$\bar{u}$	non-dimensional average fluid speed	0	reference value.

Experimental observations made by Combarnous and Bories [1] and Bories and Combarnous [18] in a saturated porous material with dimensions 66.3 × 46.3 × 5 cm indicate that a single two-dimensional cell with a horizontal axis is present for $R\cos\alpha < 4\pi^2$, where α is the tilt angle and R the Darcy–Rayleigh number. Larger Darcy–Rayleigh numbers, however, present a variety of flow modes. These authors report hexagonal cells similar to the Bénard–Rayleigh cells for $\alpha < 15°$ and $40 < R < 250$. Multiple longitudinal cells with axes parallel to the top and bottom walls, and therefore tilted with respect to the horizontal, were found for $4\pi^2 < R\cos\alpha < 240$. The frontiers separating the different modes are transition regions rather than sharply defined boundaries. A rectangular box with aspect ratio of approximately three was used by Kaneko *et al.* [19] to observe the convective flow in a tilted porous medium with isothermal boundary conditions. They reported multiple transversal (presumably bidimensional) cells with horizontal axes for $\alpha < 15°$. A single bidimensional cell appeared for $\alpha > 15°$.

The objective of the present work is to analyze numerically the behavior of natural convection flows in rectangular tilted porous materials with two-dimensional flow patterns, with special emphasis on the transition between the different cellular patterns. The study is also concerned with multiple steady-state solutions in the rectangular porous material. Recently, it has been demonstrated that some one-dimensional natural convective flows may also show two steady-state solutions in opposite directions. The stability of such solutions depends on the particular operating conditions. See, for instance, Damerell and Schoenhals [20] or Sen *et al.* [21]. This multiplicity is not merely theoretical as there is experimental evidence for two different stably convective flows under identical heating and geometrical conditions [22]. Multiple solutions for natural convective flows in rectangular bidimensional fluid filled cavities have been discussed among others by Daniels [23] and Hall and Walton [24, 25].

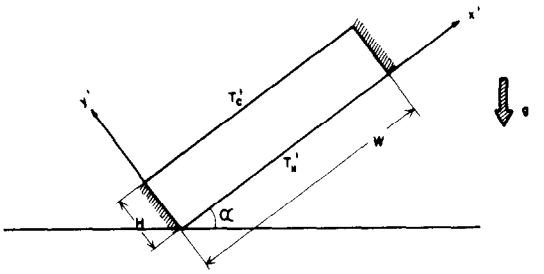

FIG. 1. The tilted porous material.

2. GOVERNING EQUATIONS AND NUMERICAL METHOD

Consider the flow of a Newtonian fluid inside a rectangular porous material as depicted in Fig. 1. Here T'_H and T'_C represent the temperature of the hot and cold walls, respectively, while the other two walls are adiabatic. The material is tilted at an angle α with respect to the horizontal plane, and is H units high and W units wide. The fluid and the porous medium are treated as a homogeneous, isotropic system with an equivalent heat conductivity.

We will analyze the steady state, using Darcy's law along with the Boussinesq approximation. The density is taken to be a linear function of the temperature.

The non-dimensional form of the governing equations in terms of the stream function Ψ and temperature T are

$$\frac{\partial^2\Psi}{\partial x^2} + D^2\frac{\partial^2\Psi}{\partial y^2} = R\left[\frac{\partial T}{\partial x}\cos\alpha - D\frac{\partial T}{\partial y}\sin\alpha\right] \quad (1)$$

and

$$\frac{\partial\Psi}{\partial y}\frac{\partial T}{\partial x} - \frac{\partial\Psi}{\partial x}\frac{\partial T}{\partial y} = \frac{1}{D^2}\frac{\partial^2 T}{\partial x^2} + \frac{\partial^2 T}{\partial y^2} \quad (2)$$

where the non-dimensional variables are defined by

$$x = x'/W, \qquad y = y'/H,$$
$$\Psi = \Psi' H/kW, \qquad T = \frac{T' - T'_C}{T'_H - T'_C}. \quad (3)$$

All variables have their usual meanings and are defined in the Nomenclature. The governing parameters are the Darcy–Rayleigh number

$$R = Kg\beta(T'_H - T'_C)H\rho_0/k\mu \quad (4)$$

the aspect ratio

$$D = W/H \quad (5)$$

and the tilt angle α.

The non-dimensional boundary conditions are

$$\begin{aligned} &\Psi = 0 && \text{on the boundaries} \\ &T = 1 && \text{for } y = 0 \text{ and } 0 \le x \le 1 \\ &T = 0 && \text{for } y = 1 \text{ and } 0 \le x \le 1 \\ &\frac{\partial T}{\partial x} = 0 && \text{for } x = 0, 1 \text{ and } 0 < y < 1. \end{aligned} \quad (6)$$

The non-dimensional heat-transfer coefficient is given by the Nusselt number defined as:

(a) local

$$Nu(x) = \partial T/\partial y; \quad (7)$$

(b) global

$$\overline{Nu} = \int_0^1 \frac{\partial T}{\partial y}\,dx. \quad (8)$$

The solution to the system of equations (1) and (2) with boundary conditions (6) was obtained using a standard finite difference numerical method. The first-order derivatives were approximated by central differences and second-order approximations were used for the derivatives in the boundary conditions. The temperature field was first found by solving equation (2) using a false transient explicit method and assuming known initial Ψ and T fields. Once the temperature had been determined, equation (1) was solved using the overrelaxation iterative scheme used by Wilkes and Churchill [26]. The Ψ values so obtained were used in equation (2) together with the more recently calculated temperature field to obtain new values for the temperature. The iterative cycle was repeated until a convergence criterion of 0.1% was satisfied. The difference between the global Nusselt numbers at the hot and cold walls was within 0.1%.

The convergence of the numerical solution with respect to the mesh fineness is shown in Tables 1 and 2. Numerical results are given in Table 1 for $D = 1$, $R = 10$ and 100 and for tilt angles of 0°, 45° and 90°. It is seen from this table that the larger the Darcy–Rayleigh number, the finer the mesh required. The $\overline{Nu}$ difference between the 30×30 and 40×40 meshes is at most 2.5% (for $\alpha = 90°$). The global Nusselt number for $\alpha = 90°$ and $R = 100$ obtained with the finer mesh is 7% smaller than that reported by Prasad and Kulacki [27] and Walker and Homsy [28]. The difference is smaller for smaller R. Balancing both precision and computational expense, the results obtained with the 30×30 mesh reported in this paper for the case $D = 1$ are considered satisfactory. The influence of the mesh on the solution for $D > 1$ is given in Table 2 for $\alpha = 0°$ and $R = 100$. We explored the effect of the increase of the number of mesh points in the x- and y-directions. The results indicate that equidistant meshes with $20 \times 10D$ points give accurate enough results with reasonable computer processing time.

3. CONVECTIVE MODES

An obvious characteristic of convection in the porous material is the appearance of single or multiple cell flows. It must be remarked that whenever we refer to multiple cells, we mean multiple two-dimensional transverse cells and not the three-dimensional longitudinal cells described by Bories and Combarnous [18]. For future reference, it is convenient to introduce a formal definition of a convection cell. The physical notion of a cell is associated with an identifiable body of fluid rotating in the same sense. Therefore, it has to be bounded by a closed streamline within which the vorticity is of the same sign.

Depending on the aspect ratio (D), the tilt angle (α) and the Darcy–Rayleigh number (R), single or multiple cell convection was found. For $D = 1$ and in the ranges $0° \le \alpha \le 180°$ and $R < 100$ the single cell mode was obtained. An example of this flow is given in Fig. 2 where the streamlines and isotherms are shown for $\alpha = 30°$ and $R = 100$. The features presented are qualitatively similar to those found in a fluid filled cavity as discussed by Ozoe *et al.* [10]. The stream function shows a single extremum value whose magnitude becomes larger as R increases, indicating a more vigorous motion, as expected. As a function of the tilt angle, the Ψ extremum value presents a maximum around 50°. This effect is discussed in detail in Section 4.

Geometries with aspect ratios greater than unity present a greater variety of convective modes. In particular, Fig. 3 shows the regions in the α,R space where the flow presents single or multiple cell modes for $D = 3$. Single cell convection takes place for

Table 1. Convergence of the numerical solution as a function of the mesh size for $D = 1$. $\overline{Nu}$ is the global Nusselt number and Ψ_m the extremum value of the stream function

Rayleigh number (R)	Mesh points	$\alpha = 0°$ $\overline{Nu}$	$\alpha = 0°$ Ψ_m	$\alpha = 45°$ $\overline{Nu}$	$\alpha = 45°$ Ψ_m	$\alpha = 90°$ $\overline{Nu}$	$\alpha = 90°$ Ψ_m
10	10 × 10	1.000	0.0000	1.031	0.5976	1.044	0.7182
	20 × 20	1.000	0.0000	1.043	0.6136	1.059	0.7198
	30 × 30	1.000	0.0000	1.048	0.6187	1.065	0.7196
100	20 × 20	2.391	5.128	3.316	6.470	2.662	4.718
	30 × 30	2.475	5.211	3.481	6.529	2.801	4.727
	40 × 40	2.517	2.252	3.564	6.552	2.873	4.728

Table 2. Convergence of the numerical solution as a function of the mesh size for $\alpha = 0°$ and $R = 100$. $\overline{Nu}$ is the global Nusselt number and Ψ_m the maximum value of the stream function

D	Mesh points	$\overline{Nu}$	Ψ_m
2	10 × 20	2.275	1.748
	10 × 40	2.442	1.950
	20 × 40	2.464	1.941
4	10 × 40	2.515	1.215
	10 × 80	2.582	1.265
	20 × 40	2.539	1.205
8	10 × 40	2.401	0.637
	10 × 80	2.504	0.563
	20 × 80	2.530	0.559

$0 < R < 200$ and tilt angles larger than approximately 50°. Two different flow patterns appear for smaller tilt angles, namely, one main cell with secondary cells developing within, and three cells circulating in alternate directions. For the parameter ranges explored, more than three cells were never found. The hatched region in Fig. 3 has $\overline{Nu} < 1.1$ and is characterized by very small flow velocity, and conduction dominated heat transfer. Along the broken line, the interface between the different cellular regions is difficult to determine, being highly sensitive to the external parameters. Typical isotherms and streamlines for $R = 100$ and $\alpha = 40°$, 25° and 10° are shown in Figs. 4–6. The first example presents a single cell where all the fluid inside the porous material circulates in the same sense and the stream function has only one extremum value. As the tilt angle is reduced, the Ψ extremum point splits in two. Parcels of rotating fluid remain isolated in the vicinity of the local extremum points, but still the whole body of fluid rotates in the same sense, driven by the main cell. This is a typical one main cell plus secondary cell convection mode. As the tilt angle is further reduced to 10°, three clearly identifiable isolated regions or cells develop with alternate directions of rotation. Three local extremum values for Ψ are found in this case.

The map of the convective modes for a two-dimensional porous material with an aspect ratio of ten is given in Fig. 7. Essentially, it presents transition characteristics similar to those found for $D = 3$, the main difference being that one, seven and nine cell convection can now be found, the larger number of cells corresponding to smaller tilt angles. The isotherms and stream function fields are shown for three typical cases in Figs. 8–10. The evolution from single cell convection at large tilt angles to multiple cells at small tilt angles is similar to that found in the $D = 3$ case.

Bories and Combarnous [18] reported an experimentally found α,R map for a three-dimensional box in which they show single two-dimensional transverse cells for $R\cos\alpha < 4\pi^2$ and a variety of three-dimensional patterns for the $R\cos\alpha > 4\pi^2$ region. In particular, for tilt angles smaller than 15° they encountered three-dimensional hexagonal cells. The numerical results presented here closely predict the appearance of the single two-dimensional cell in the region $R\cos\alpha < 4\pi^2$ and is obviously unable to predict the three-dimensional patterns.

4. PHYSICAL DESCRIPTION

We can visualize the convection pattern in a cell as being composed of a number of variable-area closed stream tubes. Heat is transferred in and out of these tubes through their imaginary walls by conduction. Also, heat is transferred along the direction of the axis mainly by convection. Near the hot wall, the heat balance in the tube is positive, i.e. more heat enters the tube through the walls than leaves it. The net energy gain is conveyed towards the cooler wall where a net amount of heat is withdrawn from the tube through its walls, completing in this manner the heat transfer. Therefore, the heat transferred globally through the porous material depends on two effects: first, the heat conducted through the imaginary walls of the tube and second, convection of the fluid moving within. Although the two effects are necessarily coupled, for purposes of clarity we will discuss them separately. The heat conducted through the tube walls depends mainly on the effective heat conductivity of the working fluid–porous medium system, and the temperature gradient in the direction perpendicular to the walls of the stream tubes. Taking the single cell in Fig. 2 as an example, we find that heat conduction is more effective downstream of the

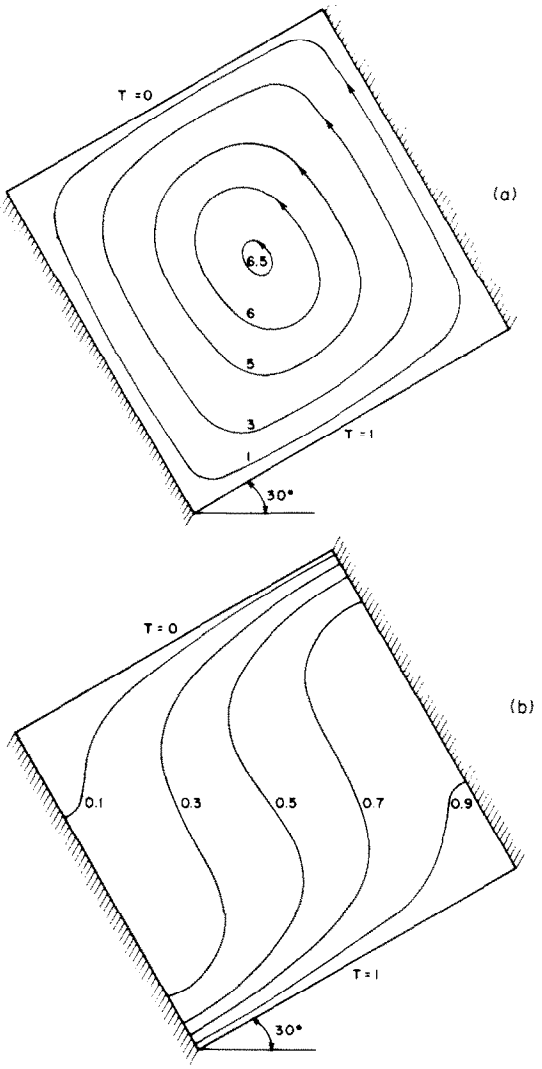

FIG. 2. (a) Streamlines and (b) isotherms for $D = 1$, $R = 100$, $\alpha = 30°$.

upper- and lower-most corners where the temperature gradients are larger. This effect is due to the deformation of the isothermal lines from their conductive pattern provoked by the motion of the fluid.

In order to gain insight into the physical nature of the flow, we consider a single stream tube. The driving force of the fluid motion inside the stream tube, and indeed in the whole of the cavity (since the choice of the stream tube is arbitrary), comes from the product of the density and the local component of the gravity acceleration vector in the direction of the stream tube. This is easily shown by considering the Darcy equation describing the momentum balance written for a coordinate η' that runs along the centerline of the stream tube, i.e.

$$w' = -\frac{K}{\mu}\left(\frac{dp'}{d\eta'} + \rho\tilde{g}\right) \tag{9}$$

where w' is the velocity in the direction of the coordinate η' and $\tilde{g}$ is the local component of the gravity acceleration vector in the η'-direction. Upon making the approximation that the stream tube has constant cross section, the mass balance indicates that w' is constant along the stream tube. Integrating along the stream tube loop, the pressure term is eliminated and we obtain

$$w' = -\frac{K}{L\mu}\int_0^L \rho\tilde{g}\,d\eta' \tag{10}$$

where L is the total length of the tube. In terms of the temperature, this expression becomes

$$w' = \frac{K\rho_0\beta}{L\mu}\int_0^L T'\tilde{g}\,d\eta' \tag{11}$$

where we have used the fact that

$$\int_0^L \tilde{g}\,d\eta' = 0.$$

The non-dimensional form of the above expression is

$$w = R\int_0^1 T(\eta)\delta(\eta)\,d\eta \tag{12}$$

where $\delta = \tilde{g}/g$, $\eta = \eta'/L$ and $w = w'H/k$. The Darcy–

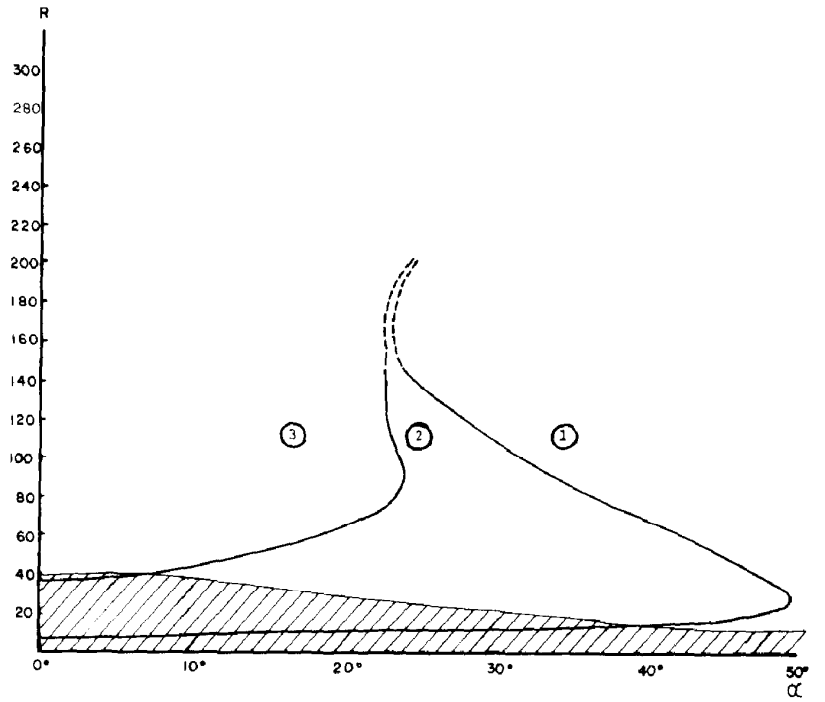

FIG. 3. Map of qualitative behavior for $D = 3$. ① Single cell; ② one cell plus secondary cells; ③ multiple cells.

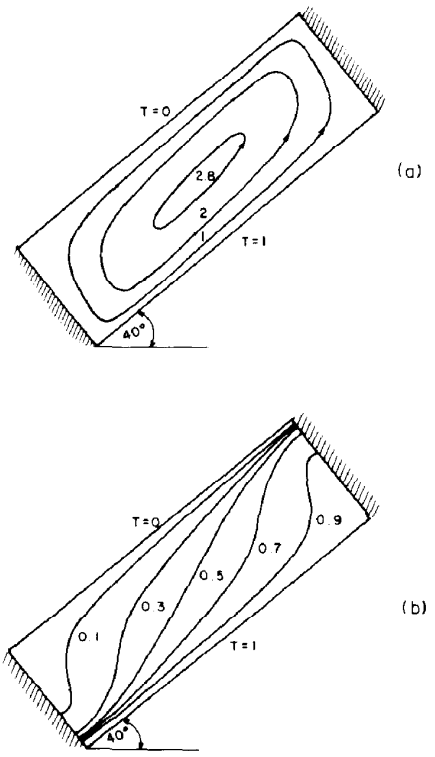

FIG. 4. (a) Streamlines and (b) isotherms for $D = 3$, $R = 100$, $\alpha = 40°$.

Rayleigh number comes out naturally as the coefficient of the buoyancy driving force along the stream tube. Due to the constant area stream tube approximation, the left- and right-hand sides of equation (12) were found to agree only within 10% for $D = 1$, $R = 100$, $\alpha = 30°$.

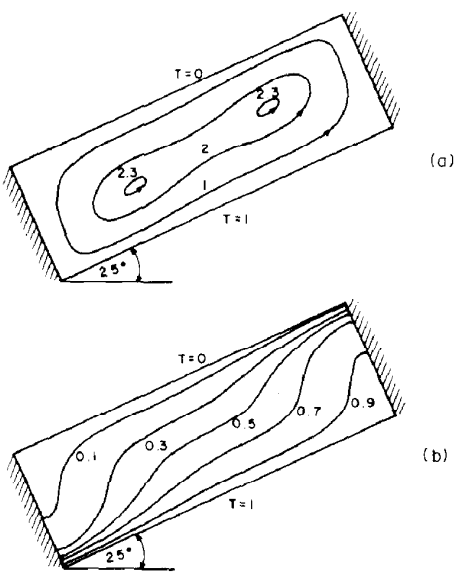

FIG. 5. (a) Streamlines and (b) isotherms for $D = 3$, $R = 100$, $\alpha = 25°$.

For unit aspect ratio, and fixed Darcy–Rayleigh number the motion of the fluid inside the porous material is most vigorous for tilt angles of approximately 50°, the precise value being dependent on R. This feature can be clearly seen From Fig. 11 where the average fluid speed $\bar{u}$ over the area A of the rectangular porous material, defined as

$$\bar{u} = \int_A (u^2 + v^2)\,dA$$

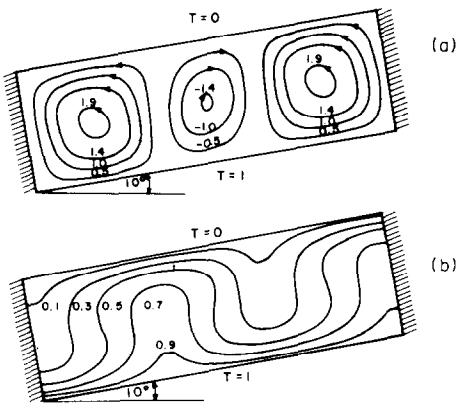

FIG. 6. (a) Streamlines and (b) isotherms for $D = 3$, $R = 100$, $\alpha = 10°$.

is plotted as a function of the tilt angle for different values of the Darcy–Rayleigh number. As shown in equation (12), the driving force is the result of the combined effects of the temperature difference and the local component of the gravity acceleration vector; therefore, the appearance of the maximum in the average speed as a function of the tilt angle can be qualitatively understood as follows: we consider the horizontal case and assume that the flow is in the counterclockwise direction. For the sake of argument, choose a particular stream tube close to the boundaries, the right-hand side branch of which is hotter (and therefore less dense) than the average, after picking up heat at the lower boundary. Likewise, the branch on the left-hand side is cooler than the average. In the two vertical branches, the gravity vector is

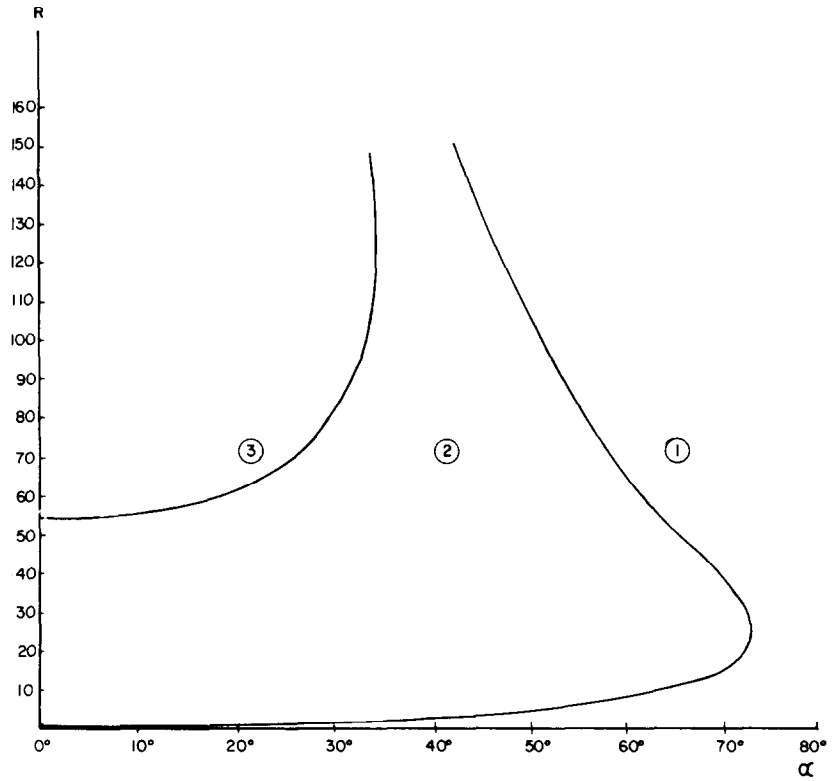

FIG. 7. Map of qualitative behavior for $D = 10$. ① One cell; ② one cell plus secondary cells; ③ multiple cells.

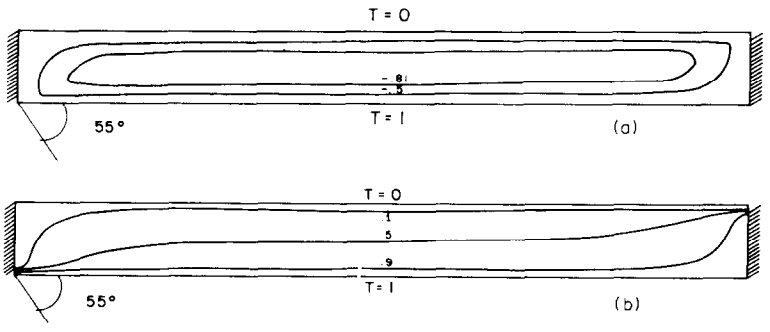

FIG. 8. (a) Streamlines and (b) isotherms for $D = 10$, $R = 100$, $\alpha = 55°$.

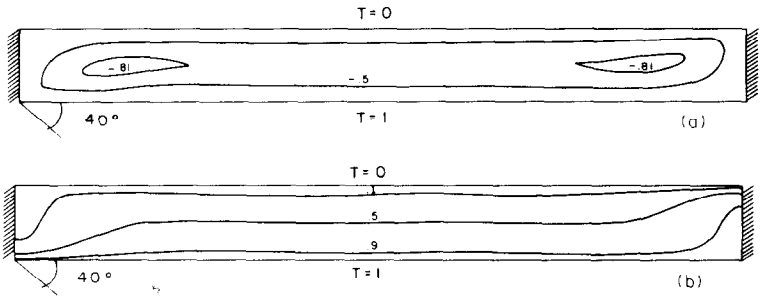

FIG. 9. (a) Streamlines and (b) isotherms for $D = 10$, $R = 100$, $\alpha = 40°$.

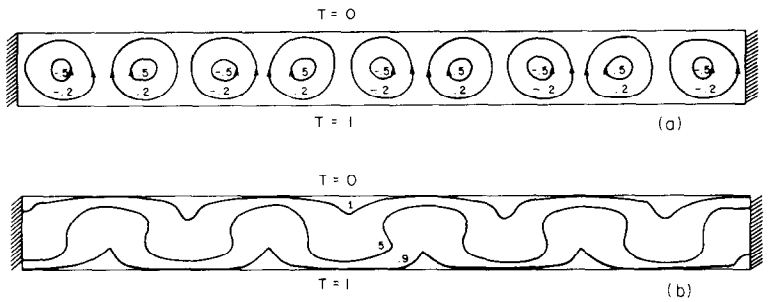

FIG. 10. (a) Streamlines and (b) isotherms for $D = 10$, $R = 100$, $\alpha = 0°$.

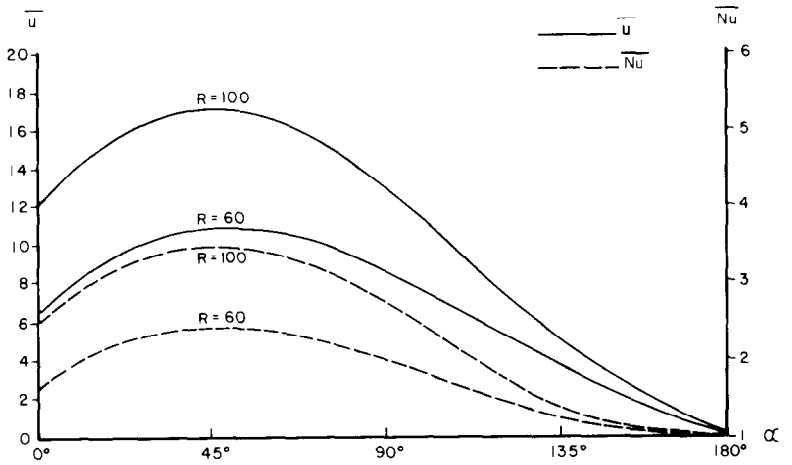

FIG. 11. Fluid average speed $\bar{u}$ and $\overline{Nu}$ as functions of tilt angle α, $D = 1$.

aligned with the stream tube and the density imbalance helps the circulation of the fluid inside the cavity as indicated by a contribution to the integral in equation (12). However, no matter what the temperature of the fluid inside the horizontal branches is, their density difference does not contribute to the integral in equation (12) since δ is zero in these branches. A similar situation is found for the vertical case. However, at an intermediate inclination the temperature differences in the fluid in all four branches of the stream tube contribute to the driving force since in each of them the component of the gravity vector is nonzero. Thus the maximum average speed can be expected at an intermediate α, between the horizontal and vertical extremes. This result reflects itself in the heat transfer results also as discussed in the next section.

5. HEAT TRANSFER RESULTS

The regions on the wall that participate more effectively in the heat transfer process can be identified using the local Nusselt number. This is shown for the lower wall in Figs. 12 and 13 for $R = 100$ and tilt angles of 10° and 60°, respectively. It is clearly seen

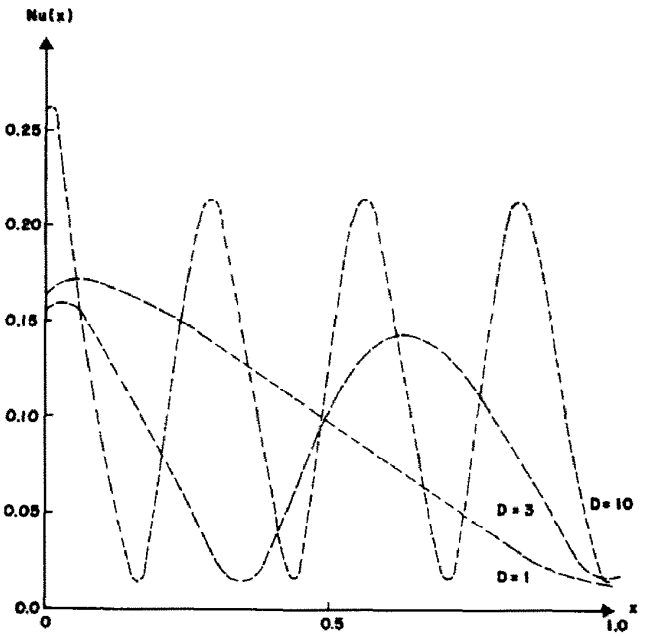

FIG. 12. Spatial variation of the local Nusselt number for $R = 100$, $\alpha = 10°$.

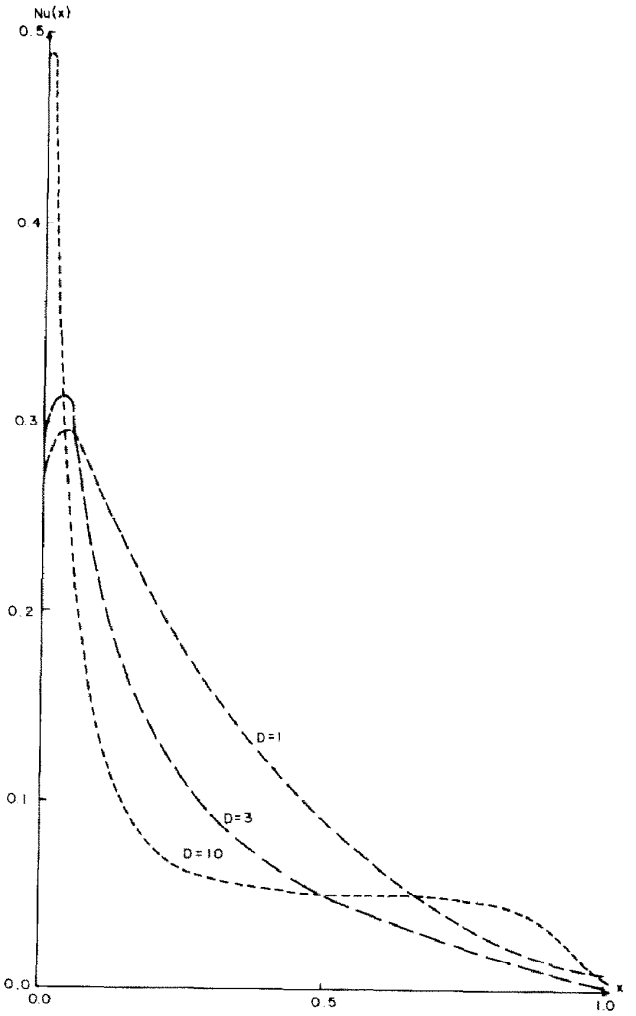

FIG. 13. Spatial variation of the local Nusselt number for $R = 100$, $\alpha = 60°$.

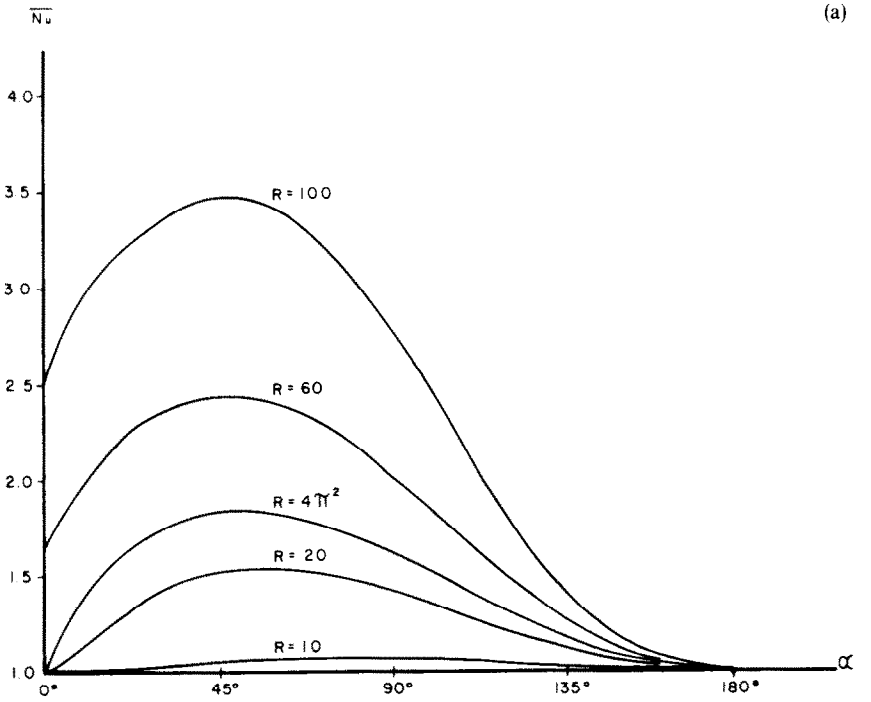
(a)
$\overline{Nu}$
4.0
3.5
3.0
2.5
2.0
1.5
1.0
R = 100
R = 60
R = 4π²
R = 20
R = 10
0°
45°
90°
135°
180°
α

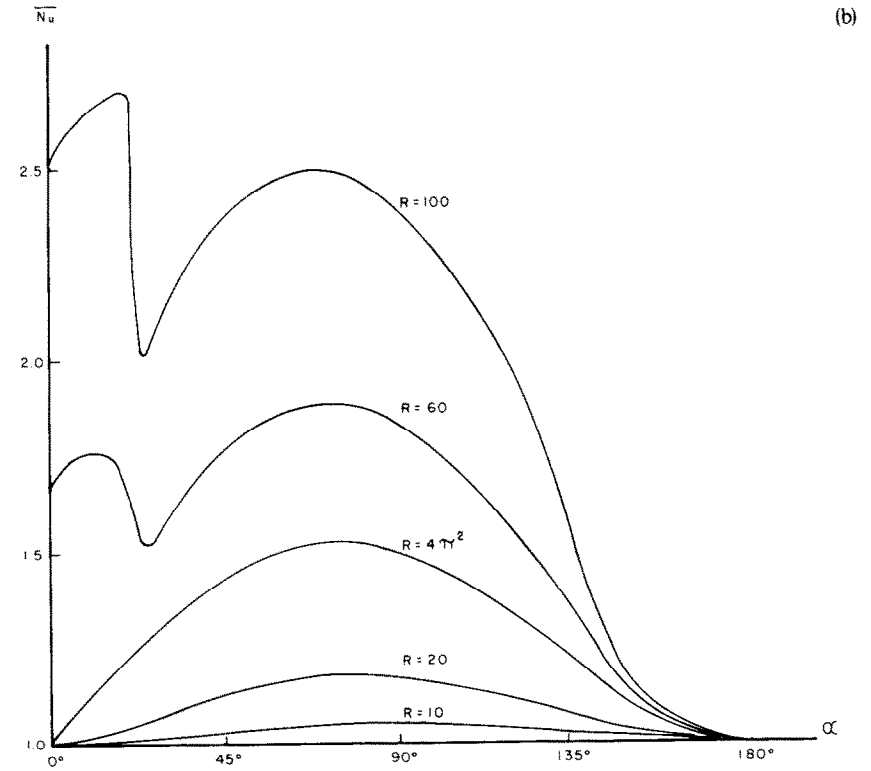
(b)
$\overline{Nu}$
2.5
2.0
1.5
1.0
R = 100
R = 60
R = 4π²
R = 20
R = 10
0°
45°
90°
135°
180°
α

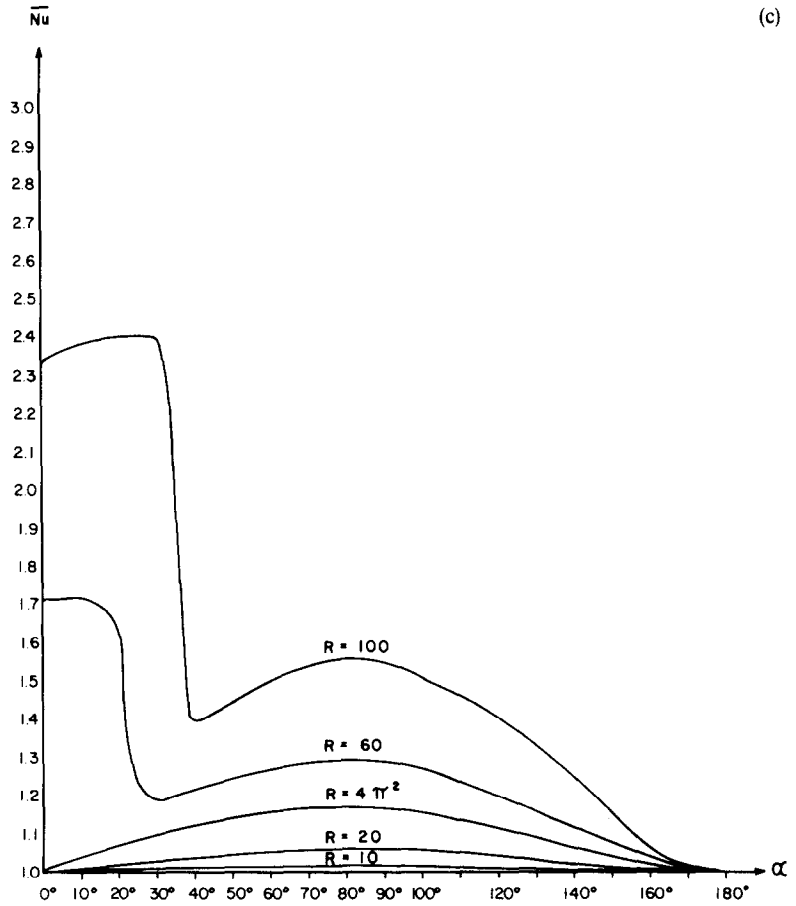

FIG. 14. Variation of global Nusselt numbers with α for: (a) $D = 1$, (b) $D = 3$, (c) $D = 10$.

that for the single cell mode, which corresponds to the $D = 1$ curve shown in Fig. 12 and all curves shown in Fig. 13, most of the heat is transferred at the corners of the material. When multiple cell convection is present, as in $D = 3$ and 10 in Fig. 12, most of the heat is transferred at several localized spots at the walls. These correspond to the boundaries between the cells where the flow is directly from the hot to the cold wall. Flow in the opposite direction leads to a minimum point in the $Nu(x)$ curve. It is found that the presence of multiple cells has the overall effect of increasing the heat transfer.

The global Nusselt number ($\overline{Nu}$) for aspect ratios of one, three and ten and for several Darcy–Rayleigh numbers are shown in Figs. 14(a)–(c), respectively, as functions of the tilt angle. The curves for unit aspect ratio present a single maximum at a tilt angle of approximately 50°. This coincides qualitatively with the fact that the most vigorous convective flow is developed at approximately this inclination. The global Nusselt number is 15% smaller than that found by Vlasuk [8] (for $R = 100$). The curves for aspect ratios 3 and 10 (Figs. 14(b) and (c), respectively) feature two local maxima, the first one for tilt angles smaller than 35°, and a second one for larger inclinations. The appearance of the latter is explained in the light of the arguments given for $D = 1$ since a single cell is present. The first maximum is, however, characteristic of the $D \neq 1$ geometry and is due to the multiple cell convection. Similar results have been obtained in a recent paper by Caltagirone and Bories [17]. Their angles for transition to single cell motion are shown in Table 3, together with those found here. The transition for $R = 100$ is much more sudden and clearly identifiable than that for $R = 60$. This is due to the fact that, as can be seen from Fig. 3, the one main cell plus secondary cell transition zone between multiple and single cell motions is much smaller for larger R.

Table 3. Transition angle from multiple to single cell convection patterns

	Aspect ratio	R	Transition angle
Caltagirone and Bories [17]	2	100	10
	4	100	29
	8	100	32
Present work	3	60	25
	3	100	25
	10	60	25
	10	100	30

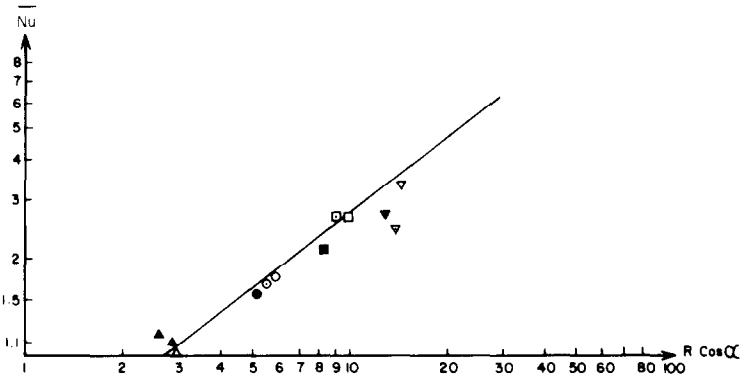

FIG. 15. Global Nusselt number as a function of $R\cos\alpha$ for $D = 3$. Continuous line is from ref. [19]. $\Delta, \alpha = 10°$, $R = 30$; $\triangle, \alpha = 20°$, $R = 30$; $\blacktriangle, \alpha = 30°$, $R = 30$; $\bigcirc, \alpha = 10°$, $R = 60$; $\odot, \alpha = 20°$, $R = 60$; $\bullet, \alpha = 30°$, $R = 60$; $\square, \alpha = 10°$, $R = 100$; $\boxdot, \alpha = 20°$, $R = 100$; $\blacksquare, \alpha = 30°$, $R = 100$; $\triangledown, \alpha = 10°$, $R = 150$; $\triangledown, \alpha = 20°$, $R = 150$; $\blacktriangledown, \alpha = 30°$, $R = 150$.

In general, the curves in Fig. 14 are difficult to correlate into a sufficiently simple expression of the form $\overline{Nu}(D, R, \alpha)$ as has been done for vertical geometries [27]. The following simplified version has also been used

$$\overline{Nu} = \overline{Nu}(D, R\cos\alpha). \tag{13}$$

Such correlations may be valid over a range where the cellular convection pattern does not change, and should not be extrapolated beyond the transition boundaries.

Experimental data for global heat transfer in a box with isothermal walls with an aspect ratio of approximately 3 were reported by Kaneko *et al.* [19]. They suggested the relation $\overline{Nu} = 0.082(R\cos\alpha)^{0.76}$ and emphasized that it had been obtained for tilt angles in the range $10° < \alpha < 30°$. These experimental results are shown as a continuous line in Fig. 15 which is compared with the values obtained here. It is clearly seen that the results are in good agreement whenever a multiple cell mode (or one cell with large secondary cells) is present, as for $R \leq 100$ and $R = 150$, $\alpha = 20°$. However, for larger tilt angles, when the single cell mode is present, the numerical result is approximately 30% smaller than the recommended empirical relation. On physical grounds it seems reasonable that single cell heat transfer, having less heat transfer channels, be smaller than that due to multiple cells if either structure could exist under identical conditions. Thus the two qualitatively different behaviors cannot be uniquely correlated. Although it is not explicitly stated in ref. [19], it appears that the experimental results were obtained for multiple cell convection.

Heat transfer results similar to those presented in this paper were recently published by Caltagirone and Bories [17]. We used our numerical method to obtain results in the conditions given in ref. [17]. The geometries $D = 2, 4$ and 8 were analyzed for $R = 100$. Global Nusselt numbers and the number of cells are given in Table 4. The agreement is satisfactory, since the difference is, except in two cases, less than 5%.

Table 4. Global Nusselt number and number of cells for $R = 100$

		This work		Caltagirone and Bories [17]		
D	α	Number of cells	$\overline{Nu}$	Number of cells	$\overline{Nu}$	Difference in $\overline{Nu}$ (%)
2	0	3	2.46	3	2.65	7
	5	3	2.53	3	2.64	4
	10	3	2.55	3	2.60	2
	15	1	2.39	1	2.44	2
4	0	5	2.54	5	2.67	5
	10	5	2.60	5	2.69	3
	20	3	2.57	3	2.62	2
	30	3	2.60	1	2.57	1
	40	1	2.00	1	2.02	1
8	0	11	2.53	11	2.64	4
	10	11	2.53	9	2.70	6
	20	9	2.58	9	2.67	3
	30	5	2.35	5	2.45	4
	40	1 + sec	1.50	—	1.52	1
	50	1 + sec	1.57	—	1.57	0

6. MULTIPLE SOLUTIONS FOR A SQUARE MATERIAL

The existence of multiple steady-state solutions, in the present bidimensional analysis can be easily demonstrated for the horizontal case. Consider the governing equations, equations (1) and (2), and the boundary conditions, equation (6), for $D = 1$ and $\alpha = 0°$.

Assume that $\Psi(x, y)$ and $T(x, y)$ are solutions to the system, then $-\Psi(x, y)$ and $T(-x, y)$ are also. Moreover, it should be remarked that the conductive solution, namely $\Psi(x, y) = 0$ and $T = 1 - y$, always satisfies the governing equations and boundary conditions for $\alpha = 0°$. Therefore, for the horizontal case,

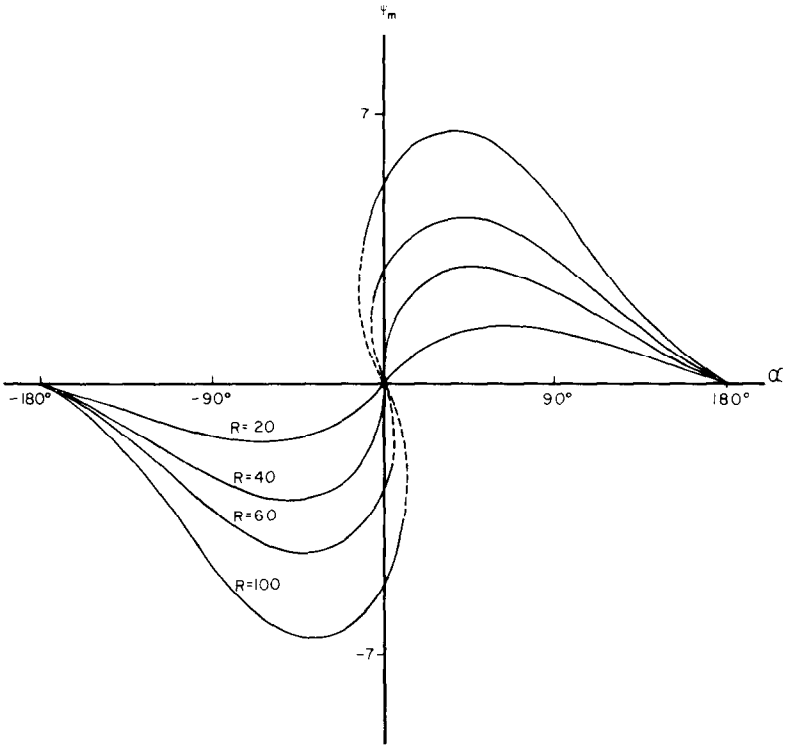

FIG. 16. Ψ_m as a function of α for $D = 1$.

there can be either one or three solutions depending on whether $R < 4\pi^2$ or $R > 4\pi^2$.

The multiplicity of steady-state solutions also exists for slightly inclined porous materials, as has been analytically investigated by Walch and Dulieu [13, 14]. Here, this kind of behavior is investigated numerically. In order to characterize the flow we shall use the variable Ψ_m defined by

$$\Psi_m = \pm \max|\Psi(x, y)| \tag{14}$$

where the positive and negative signs are taken for counterclockwise and clockwise circulation, respectively.

Figure 16 shows Ψ_m as a function of the tilt angle as obtained from the numerical solution for different Darcy–Rayleigh numbers. Curves for $R < 4\pi^2$ present only one solution for any α. In contrast, the curves for $R > 4\pi^2$ show a region around $\alpha = 0°$ where three solutions are possible.

Two different solutions could be obtained with the numerical algorithm for $R > 4\pi^2$ by using different initial stream function and temperature fields for the iterations. Using $\Psi = T = 0$ as the initial values for the entire region of integration, we get the counterclockwise solutions for positive tilt angles and clockwise solutions for negative tilt angles. These can be referred to as the 'natural' solutions as defined by Walch and Dulieu [14], who described this phenomenon using a small tilt angle approximation. Using these results as starting values, two counter rotating solutions were obtained for zero tilt angle. Repeating the procedure, we could go to counterclockwise (clockwise) rotating solutions for small negative (positive) tilt angles. These are the 'antinatural' solutions. Thus, there is an interval in the vicinity of $\alpha = 0°$ for which multiple solutions could be found. The size of the interval depends on the Darcy–Rayleigh number, increasing with R. For example, for $R = 60$ multiple solutions can be obtained in the range $-4° < \alpha < 4°$, while for $R = 100$ the range increases to $-10° < \alpha < 10°$. Results found with the numerical procedure are shown with continuous lines in Fig. 16. The curves are completed with broken lines, considering the fact that the origin is always a solution. It seems that the solutions shown by broken lines, are unstable [29], but this point cannot be further explored with the methods described in this paper. The first and third quadrants represent the natural solutions and the other two the antinatural circulation. The streamlines and isotherms for the counterclockwise (natural) and clockwise (antinatural) circulation for $D = 1$, $R = 100$ and $\alpha = 5°$, are shown in Fig. 17. In Fig. 17(a), the fluid moves upwards near the hot wall and downwards near the cold wall. In Fig. 17(b), the fluid descends near the hot wall and ascends near the cold wall. Close scrutiny of the temperature field shows that, in both cases, the ascending stream is hotter than the descending one, providing the driving force in the respective direction of motion. This explains the existence of two counter rotating solutions, even though at first sight, the second solution might seem to be unrealistic. Reference can be made to a study of one-dimensional

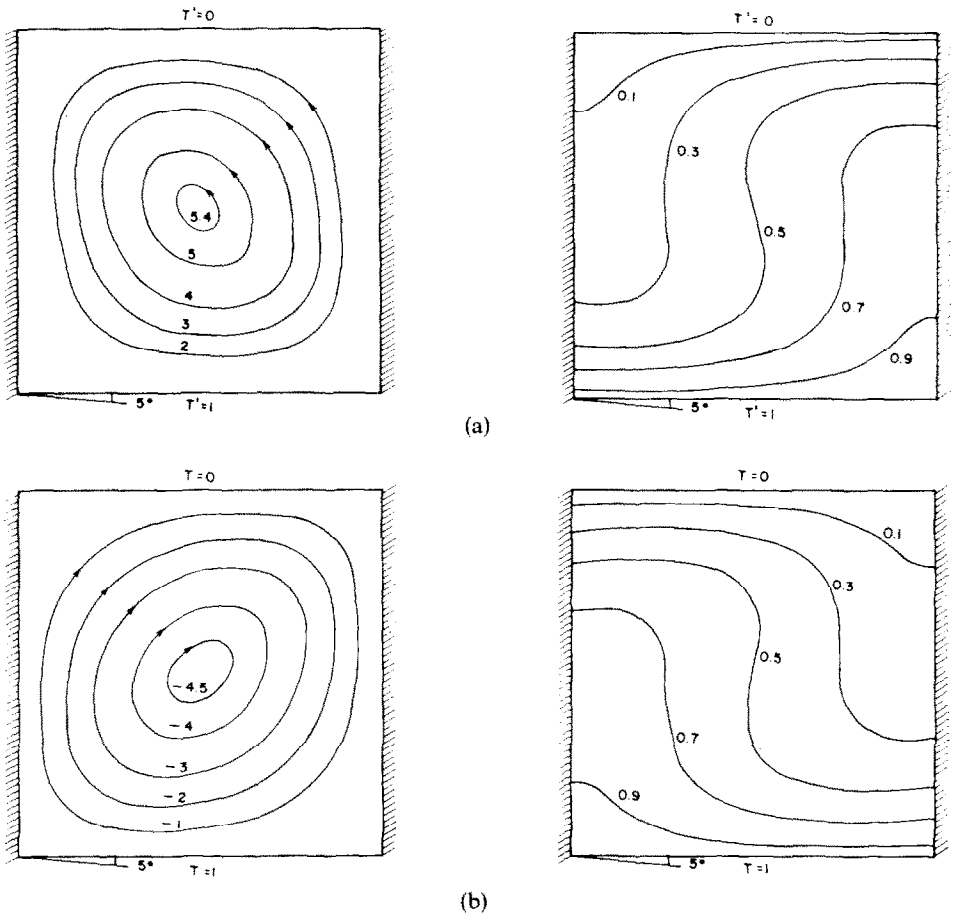

FIG. 17. Streamlines and isotherms for (a) counterclockwise and (b) clockwise circulation for $D = 1$, $R = 100$, $\alpha = 5°$.

thermosyphon models (see ref. [30]) where a similar situation is encountered. It is to be emphasized that the natural convection equations considered as an initial value problem have a unique solution. However, different initial conditions can lead to different steady-state flows. A horizontal porous material with a clockwise convection cell can be carefully tilted a small positive angle, with the cell maintaining the same flow direction. This is the antinatural motion. If heating were applied from rest for this same positive angle, natural counterclockwise motion would have resulted. The adjective natural is thus used to describe the flow which would develop on starting from rest conditions. This is the solution that is usually investigated.

7. CONCLUSIONS AND DISCUSSION

The phenomenon of natural convection in a two-dimensional porous material saturated with fluid was studied by means of a numerical method. Conduction, single or multiple cell convection take place depending on the aspect ratio, Darcy–Rayleigh number and tilt angle. For zero tilt angle and $R < 4\pi^2$, the heat transfer is purely conductive, while for $R > 4\pi^2$ the main heat transfer mode is convection. The $\alpha = 0°$ mathematical model is structurally unstable. In other words, for $\alpha \neq 0°$ behavior of the natural convection system is completely different, however small α might be. When the porous material is tilted, both conduction and convection modes are present for all Darcy–Rayleigh numbers.

Flow in square material was found to feature one cell, regardless of the tilt angle in the Darcy–Rayleigh number range explored. The maximum average velocity and the maximum global heat transfer take place at approximately the same tilt angle, indicating the importance of the fluid motion on the heat transfer.

When the aspect ratio is larger than unity, single or multiple cell convection can take place. Multiple cell convection augments the heat transferred through the porous material since the main mechanism of heat exchange is due to the motion of the fluid in a direction perpendicular to the isothermal walls. In the single cell mode this occurs only in regions close to the isothermal walls, while in the multiple cell convection, the fluid in the regions between adjacent

cells also moves in the direction perpendicular to the isothermal walls.

At tilt angles close to zero the preferred mode of circulation is multiple cell while at greater tilt angles, the preferred mode is single cell. The change occurs at approximately 30° for $D = 3$ and 10. This characteristic has also been reported for fluid filled cavities [10]. It was found that the maximum number of cells in the $D = 8$ case was eleven while for $D = 10$ nine cells appeared, for $\alpha = 0°$. We analyzed this point in detail, and used various meshes to try to clarify whether the number of cells depended on the mesh fineness. Meshes of 20×60, 20×80 and 20×100 were used and in no case more than nine were encountered.

The existence of the multiplicity of solutions has also been demonstrated. It was found that for a given Darcy–Rayleigh number, and a small (positive or negative) tilt angle and unit aspect ratio, there exist two steady-state solutions. In the particular case of $\alpha = 0°$ and $R > 4\pi^2$ there are three solutions, one unstable conductive and two convective with opposite circulations. It is expected that there are also three solutions for some tilt angles different from zero, the third one being unstable and therefore impossible to obtain with a numerical method. The manifold for the solutions in the Ψ_m, R, α space is hence a cusp catastrophe.

Although no exploration was made into the multiplicity of solutions for $D \neq 1$, the variety of convective patterns obtained suggests a far more complete bifurcation set, where not only the conduction to convection transition is possible but also the single to multiple cell convection, and multiple to multiple cell convection. For a fixed D, some properties can be inferred. For instance, the interfaces between different convective cell structures in the α, R space for $D = 3$ and 10 (Figs. 3 and 7) resemble a projection of the cusped catastrophe set.

Application of Thom's classification scheme for elementary catastrophes [31] to natural convection is not immediate, since infinite dimensional non-gradient type equations are involved. However, the present study clearly shows that some of its results may be used. A full study of these phenomena would involve the description of a manifold for the solutions in at least a tetradimensional space Ψ_m, R, α, D. Such a manifold would probably be identified with a higher order catastrophe.

Acknowledgement—Support from the Programa Universitario de Energía of the U.N.A.M., is gratefully acknowledged. Thanks are also due to one of the referees for making available a preprint of ref. [17].

REFERENCES

1. M. A. Combarnous and S. A. Bories, Hydrothermal convection in saturated porous media, *Adv. Hydrosci.* **10,** 231–307 (1975).
2. N. Rudraiah and T. Masuoka, Asymptotic analysis of natural convection through horizontal porous layer, *Int. J. Engng Sci.* **20,** 27–39 (1982).
3. N. Rudraiah and P. K. Sirmani, Finite amplitude cellular convection in a fluid saturated porous layer, *Proc. R. Soc. Lond.* **A373,** 199–222 (1980).
4. J. W. Elder, Steady-free convection in a porous medium heated from below, *J. Fluid Mech.* **27,** 29–48 (1967).
5. J. E. Weber, Convection in a porous medium with horizontal and vertical temperature gradients, *Int. J. Heat Mass Transfer* **17,** 241–248 (1974).
6. J. E. Weber, The boundary-layer regime for convection in a vertical porous layer, *Int. J. Heat Mass Transfer* **18,** 569–573 (1975).
7. P. J. Burns, L. C. Chow and C. L. Tien, Convection in a vertical slot filled with porous insulation, *Int. J. Heat Mass Transfer* **20,** 919–926 (1977).
8. M. P. Vlasuk, Convective heat transfer in a porous layer (in Russian), 4th All Union Heat and Mass Transfer Conf., Minsk (1972).
9. J. E. Hart, Stability of the flow in a differentially heated inclined box, *J. Fluid Mech.* **47,** 547–576 (1971).
10. H. Ozoe, K. Yamamoto, H. Sayama and S. W. Churchill, Natural convection in an inclined rectangular channel heated on one side and cooled on the opposite side, *Int. J. Heat Mass Transfer* **17,** 1209–1217 (1974).
11. P. H. Holst and K. Aziz, A theoretical and experimental study of natural convection in a confined porous medium, *Can. J. Chem. Engng* **50,** 232–241 (1972).
12. J. E. Weber, Thermal convection in a tilted porous layer, *Int. J. Heat Mass Transfer* **18,** 474–475 (1975).
13. J. P. Walch and B. Dulieu, Convection naturelle dans une boîte rectangulaire legerment inclinée contenant un milieu poreux, *Int. J. Heat Mass Transfer* **22,** 1607–1612 (1979).
14. J. P. Walch and B. Dulieu, Convection de Rayleigh–Bénard dans une cavité poreuse faiblement inclinée, *J. Phys. Lett.* **43,** L103–L107 (1982).
15. E. R. Lapwood, Convection of a fluid in a porous medium, *Proc. Camb. Phil. Soc.* **44,** 508–521 (1948).
16. J. L. Beck, Convection in a box of porous material saturated with fluid, *Physics Fluids* **15,** 1377–1383 (1972).
17. J. P. Caltagirone and S. Bories, Solutions and stability criteria of natural convective flow in an inclined porous layer, *J. Fluid Mech.* **155,** 267–287 (1985).
18. S. A. Bories and M. A. Combarnous, Natural convection in a sloping porous layer, *J. Fluid Mech.* **57,** 63–79 (1973).
19. T. Kaneko, M. F. Mohtadi and K. Aziz, An experimental study of natural convection in inclined porous media, *Int. J. Heat Mass Transfer* **17,** 485–496 (1974).
20. P. S. Damerell and R. J. Schoenhals, Flow in a toroidal thermosyphon with angular displacement of heated and cooled sections, *J. Heat Transfer* **101,** 672–676 (1979).
21. M. Sen, E. Ramos and C. Treviño, The toroidal thermosyphon with known heat flux, *Int. J. Heat Mass Transfer* **28,** 219–233 (1985).
22. R. Acosta, M. Sen and E. Ramos, Single phase natural circulation in a tilted square loop, to be published in *Wärme und Stoffübertragung.*
23. P. G. Daniels, The effect of distant sidewalls on finite amplitude Bénard convection, *Proc. R. Soc.* **A358,** 173 (1977).
24. P. Hall and I. C. Walton, Bénard convection in a finite box: secondary and imperfect bifurcations, *J. Fluid Mech.* **90,** 377–395 (1979).
25. P. Hall and I. C. Walton, The smooth transition to a convective regime in a two-dimensional box, *Proc. R. Soc.* **A358,** 199–201 (1977).
26. J. D. Wilkes and S. W. Churchill, The finite difference computation of natural convection in a rectangular enclosure, *A.I.Ch.E. Jl* **12,** 161–166 (1966).

27. V. Prasad and F. A. Kulacki, Convective heat transfer in a rectangular porous cavity—effect of aspect ratio on flow structure and heat transfer, *J. Heat Transfer* **106**, 158–165 (1984).
28. K. L. Walker and G. M. Homsy, Convection in a porous cavity, *J. Fluid Mech.* **87**, 449–474 (1978).
29. T. B. Benjamin, Bifurcation phenomena in steady flows of a viscous fluid, *Proc. R. Soc.* **A359**, 1–26 and 27–43 (1978).
30. M. Sen and C. Treviño, One-dimensional thermosyphon analysis, *Latin Am. J. Heat Mass Transfer* **7**, 135–150 (1983).
31. R. Thom, *Structural Stability and Morphogenesis.* Addison-Wesley, New York (1975).

ETUDE NUMERIQUE DE LA CONVECTION NATURELLE DANS UN MATERIAU POREUX RECTANGULAIRE ET INCLINE

Résumé—La convection naturelle bidimensionnelle dans un matériau poreux rectangulaire, incliné est analysée en résolvant numériquement les équations des bilans de masse, de quantité de mouvement, d'énergie, en utilisant la loi de Darcy et l'approximation de Boussinesq. Les conditions aux limites considérées correspondent à deux parois opposées maintenues à deux températures uniformes mais différentes et les deux autres étant thermiquement isolées. Les paramètres externes considérés sont l'angle d'inclinaison, le rapport de forme et le nombre de Darcy–Rayleigh. On trouve trois modes principaux de convection : la conduction, la convection avec un ou plusieurs cellules et leur description est donnée en détail. Les nombres de Nusselt locaux et globaux sont présentés en fonction des paramètres externes. La multiplicité des solutions est explorée pour un rapport de forme unité. L'existence de plus d'une solution est trouvée lorsque la paroi inférieure est à une température élevée et à une position horizontale ou proche de l'horizontale.

NUMERISCHE BERECHNUNG DER NATÜRLICHEN KONVEKTION IN EINEM RECHTECKIGEN GENEIGTEN PORÖSEN MATERIAL

Zusammenfassung—Die zweidimensionale natürliche Konvektionsströmung in einem geneigten rechteckigen, mit Flüssigkeit gesättigten porösen Material wird numerisch berechnet, indem die Bilanzgleichungen für Masse, Impuls und Energie mit Hilfe des Darcy-Gesetzes und der Boussinesq-Approximation gelöst werden. Isotherme Randbedingungen werden betrachtet, wobei zwei gegenüberliegende Seiten auf konstanten, jedoch verschiedenen Temperaturen gehalten werden, während die beiden anderen Seiten wärmegedämmt sind. Die betrachteten externen Parameter sind der Neigungswinkel, das Seitenverhältnis und die Darcy–Rayleigh-Zahl. Drei konvektive Hauptzustände werden gefunden: Leitung, Einzell- und Vielzellkonvektion; ihre Eigenschaften werden detailliert beschrieben. Örtliche und globale Nusselt-Zahlen werden als Funktion der externen Parameter dargestellt. Die Anzahl der Lösungen wird für ein Seitenverhältnis von eins untersucht. Liegt bei horizontaler oder nahezu horizontaler Lage die Bodentemperatur über den Wandtemperaturen, so existiert mehr als eine Lösung.

ЧИСЛЕННОЕ ИССЛЕДОВАНИЕ ЕСТЕСТВЕННОЙ КОНВЕКЦИИ В ПОРИСТОЙ СРЕДЕ, ЗАПОЛНЯЮЩЕЙ НАКЛОННУЮ ПОЛОСТЬ ПРЯМОУГОЛЬНОГО СЕЧЕНИЯ

Аннотация—На основе уравнений сохранения массы, импульса и энергии с использованием закона Дарси и приближения Буссинеска численно анализируется двумерная естественная конвекция жидкости в пористой среде, находящейся в наклонной полости прямоугольного сечения. Рассматриваются изотермические граничные условия, при которых две противоположные стенки имеют постоянную, но различную температуру, а две других являются теплоизолированными. Определяющими параметрами считаются угол наклона, отношение ширины к толщине и число Дарси–Рэлея. Обнаружены три основных режима: теплопроводности, одноячеистой конвекции, многоячеистой конвекции. Подробно рассмотрены характеристики указанных режимов. Получены зависимости локального и интегрального чисел Нуссельта от определяющих параметров. Исследуется единственность решения при отношении ширины к толщине, равном единице. Если нижняя стенка является более горячей и находится в горизонтальном или близком к нему положении, то оказывается, что решение уравнений не является единственным.